Inorg. Chem. **2007**, *46*, 2159–2166

Combined Theoretical and Experimental Analysis of the Bonding in the Heterobimetallic Cubane-Type Mo_3NiS_4 and Mo_3CuS_4 Core Clusters

Juan Andrés,[†] Marta Feliz,*[,†] Jordi Fraxedas,[‡] Victor Hernández,[§] Juan T. López-Navarrete,[§] Rosa Llusar,*[,†] Guillaume Sauthier,[‡] Fabricio R. Sensato,[†] Bernard Silvi,[⊥] Carles Bo,[||] and Josep M. Campanera[||]

Departmento de Química Física i Analítica, Universitat Jaume I, P.O. Box 224, 12080 Castelló, Spain, Institut de Ciéncia de Materials de Barcelona (ICMAB-CSIC), Campus de la Universitat Autónoma de Barcelona, E-08193 Bellaterra, Spain, Departamento de Química Física, Universidad de Málaga, 29071 Málaga, Spain, Laboratoire de Chimie Théorique (UMR 7616 CNRS), Université Pierre et Marie Curie, Paris, France, and Institute of Chemical Research of Catalonia (ICIQ), Av. Països Catalans 16, 43007 Tarragona, Spain

Received September 27, 2006

X-ray structural data for the cubane-type clusters $[Mo_3CuS_4(dmpe)_3Cl_4]^+$ and $Mo_3NiS_4(dmpe)_3Cl_4$ (dmpe = 1,2-bis(dimethylphosphino)ethane) with 16 metal electrons have been compared with optimized structural parameters calculated using "ab initio" methodologies. Compound $Mo_3NiS_4(dmpe)_3Cl_4$ crystallizes in the cubic noncentrosymmetric space group $P2_13$ with a Mo–Ni distance of 2.647 Å, that is 0.2 Å shorter than the Mo–Cu bond length in the isoelectronic copper cluster. The best agreement between theory and experiments has been obtained using the B3P86 method. In order to validate the B3P86 results, accurate infrared and Raman spectra have been acquired and the vibrational modes associated to the cubane-type $Mo_3M'S_4$ (M′ = Cu or Ni) unit have been assigned theoretically. The electronic changes taking place when incorporating the M′ into the Mo_3S_4 unit have been analyzed from a theoretical and experimental perspective. The bond dissociation energies between M′–Cl and Mo_3S_4 fragments show that formation of $[Mo_3CuS_4(dmpe)_3Cl_4]^+$ is 135 kcal/mol energetically less favorable than the Ni incorporation. The more robust nature of the Mo_3NiS_4 fragment has been confirmed by mass spectrometry. The X-ray photoelectron spectroscopy (XPS) spectra of the trimetallic and tetrametallic complexes have been measured and the obtained binding energies compared with the computed electronic populations based on topological approaches of the electron localization function (ELF). The energies and shapes of the Cu 2p and Ni 2p lines indicate formal oxidation states of Cu(I) and Ni(II). However, the reductive addition of nickel into $[Mo_3S_4(dmpe)_3Cl_3]^+$ causes a small decrease in the Mo 3d binding energies. This fact prevents an unambiguous assignment of an oxidation state in a conventional way, a circumstance that has been analyzed through the covariance of the electronic populations associated to the C(M′) core and V(Mo_3Ni) and V(S(2)′) valence basins where Mo_3NiS_4 is a particularly electronically delocalized chemical entity.

1. Introduction

The nature of the metal−metal bond in transition metal cluster complexes continues to be a topic of actual interest often associated with the potential applications of these systems as models for biological and industrial catalysts.[1] Although the initial interest of cubane-type clusters was focused on industrial hydrodesulfurization processes, especially for Mo_3NiS_4 and Mo_3CoS_4 complexes,[2,3] other catalytic applications have been envisioned for these compounds. In

* To whom correspondence should be addressed: Institut Charles Gerhardt, UMR 5253 (CNRS-UM2-ENSOM), Equipe CTMM, cc 14, Université Montpellier II, Place Eugéne Bataillon, 34000 Montpellier, France (M.F.) E-mail: marta.feliz@univ-montp2.fr (M.F.); llusar@exp.uji.es (R.L.).
[†] Universitat Jaume I.
[‡] Institut de Ciència de Materials de Barcelona.
[§] Universidad de Málaga.
[⊥] Université Pierre et Marie Curie.
[||] Institute of Chemical Research of Catalonia.

(1) Burgess, B. K.; Lowe, D. J. *Chem. Rev.* **1996**, *96*, 2983−2011.
(2) Riaz, U.; Curnow, O. J.; Curtis, M. D. *J. Am. Chem. Soc.* **1994**, *116*, 4357−4363.
(3) Herbst, K.; Monari, M.; Brorson, M. *Inorg. Chem.* **2002**, *41*, 1336−1338.

10.1021/ic061853g CCC: $37.00 © 2007 American Chemical Society
Published on Web 02/16/2007

particular $[Mo_3CuS_4(dmpe)_3Cl_4]^+$ and the enantiomerically pure cubane (*P*)-$[Mo_3CuS_4(Me\text{-}BPE)_3Cl_4]^+$ (Me-BPE = 1,2-bis[(2*R*,5*R*)-2,5-(dimethylphospholan-1-yl)]ethane) act as efficient catalysts in the intramolecular cyclization of diazo ketones and intermolecular cyclopropanation of styrene with ethyl diazo acetate.[4] On the other hand, a high catalytic activity of the cluster $[\{Mo_3NiS_4Cp^*_3\}_2(cod)](PF_6)_2$ (cod = 1,5-cyclooctadiene) has been described for the intramolecular addition of carboxylic acid to alkynes to afford enol lactones, by activation of the alkyne.[5]

Our interest has been focused on the $Mo_3M'S_4$ complexes (M′ = Cu and Ni), where the molybdenum atoms are coordinated to diphosphine ligands and the heterometal is bonded to a chloride atom. The number of metal electrons in these $[Mo_3M'S_4(diphosphine)_3Cl_4]^{0/+}$ clusters equals 16 for both copper and nickel, and the catalysis is centered at the heterometal M′. The catalytic activity of $[Mo_3CuS_4(diphosphine)_3Cl_4]^+$ is consistent with Cu(I), while some controversy exists regarding the formal oxidation state of nickel in cubane-type Mo_3NiS_4 cluster complexes. For example, the lack of activity for these nickel compounds in hydrodesulfurization processes has been attributed to the heterometal low electron density whose reactivity basically resembles that of Ni(II).[6] Although this observation agrees with the electrochemical properties and XPS measurements on these Mo_3NiS_4 clusters, theoretical investigations do not fully support this interpretation.

Molecular orbital (MO) calculations on these heterobimetallic cluster complexes support the existing ambiguity regarding the metal oxidation states assignment. In fact, the correct match between the symmetry of the orbitals associated to the metal−metal bond with the linear orbital combinations of the bridging ligand atoms makes difficult any analysis of the metal−metal bond and metal formal oxidation states based on MO methodologies.[7] In the past years topological approaches, such as the atoms in molecules (AIM) theory or the electron localization function (ELF) analysis, have emerged aimed to investigate the chemical bond as an alternative to the widely used MO interpretation, and they provide a complementary view to the standard valence analyses.[8,9] These approaches, based on the theory of dynamical systems, offer an orbital independent framework which enables a partition of the molecular space into basins of attractors bearing a chemical meaning,[10−12] and quantitative information can be further extracted by integrating the electron density over these localization basins.[13−16] On this regard, the application of topological analyses as a tool to understand the chemical bond in polynuclear metal cluster complexes has been recently reviewed by some of us.[17]

In this work, we report an extended theoretical and experimental combined study of the structural, energetic, spectroscopic (IR, Raman, XPS), electronic, and bonding properties of $[Mo_3CuS_4(dmpe)_3Cl_4]^+$ and $Mo_3NiS_4(dmpe)_3Cl_4$ with 16 metal cluster electrons. An analysis regarding the incorporation of the heterometal, Cu or Ni, into the trinuclear $[Mo_3S_4(dmpe)_3Cl_3]^+$ precursor is presented.

2. Experimental Section

Materials. The cubane-type $[Mo_3NiS_4(dmpe)_3Cl_3(CH_3CN)]PF_6$ and $[Mo_3CuS_4(dmpe)_3Cl_4]PF_6$ (dmpe = 1,2-bis(dimethylphosphino)ethane) clusters were obtained according to literature methods.[6,18] TBACl was purchased from commercial sources, and solvents were used as received.

Physical Measurements. Fourier transform infrared absorption (FTIR) spectra were recorded on a Bruker Equinox 55 spectrometer in the 7500−370 cm^{-1} range. Compounds were ground to a powder and pressed in KBr pellets. Spectra were collected with a spectral resolution of 2 cm^{-1}, and the mean of 50 scans was obtained. Interference from atmospheric water vapor was minimized by purging the instrument with dry argon prior to data collection. Raman spectra of $Mo_3NiS_4(dmpe)_3Cl_4$ were not obtained due to calcination of the product with an operating power for the exciting laser radiation of 100 mW. XPS experiments were performed at room temperature with a SPECS EA10P hemispherical analyzer using both nonmonochromatic Mg Kα (1253.6 eV) and Al Kα (1486.6 eV) lines of about 300 W in a base pressure of $\approx 10^{-9}$ mbar. The reported binding energies are determined within an error of ±0.2 eV and are referred to the 284.8 eV C1s line (adventitious carbon). Electrospray mass spectra were recorded with a Quattro LC (quadrupole−hexapole−quadrupole) mass spectrometer with an orthogonal *Z*-spray electrospray interface (Micromass, Manchester, U.K.). The cone voltage was set at 40 V unless otherwise stated using DMF as the mobile phase solvent. Nitrogen was employed as a drying and nebulizing gas. Isotope experimental patterns were compared with theoretical patterns obtained using the MassLynx 3.5 program.

X-ray Data Collection and Structure Refinement. Suitable crystals for X-ray studies of the $Mo_3NiS_4(dmpe)_3Cl_4 \cdot 0.5CH_2Cl_2$ neutral complex were grown by slow evaporation of a $[Mo_3NiS_4(dmpe)_3Cl_3(CH_3CN)]PF_6$ dichloromethane concentrated solution in presence of a TBACl excess. A dark green crystal was mounted at the top of a glass fiber with the use of epoxy cement. X-ray diffraction experiments were carried out on a Bruker SMART CCD diffractometer using Mo Kα radiation ($\lambda = 0.71073$ Å). The data were collected with a frame width of 0.3° in Ω and a counting time of 20 s per frame at a crystal to detector distance of 4 cm. The software SAINT 6.2 was used for integration of intensity reflections and scaling and SADABS for absorption correction.[19,20]

(4) Feliz, M.; Guillamon, E.; Llusar, R.; Vicent, C.; Stiriba, S. E.; Perez-Prieto, J.; Barberis, M. *Chem. Eur. J.* **2006**, *12*, 1486−1492.
(5) Takei, I.; Wakebe, Y.; Suzuki, K.; Enta, Y.; Suzuki, T.; Mizobe, Y.; Hidai, M. *Organometallics* **2003**, *22*, 4639−4641.
(6) Feliz, M.; Llusar, R.; Uriel, S.; Vicent, C.; Brorson, M.; Herbst, K. *Polyhedron* **2005**, *24*, 1212−1220.
(7) Bahn, C. S.; Tan, A.; Harris, S. *Inorg. Chem.* **1998**, *37*, 2770−2778.
(8) Bader, R. F. W. *Atoms in Molecules: A Quantum Theory*; Oxford University Press: Oxford, 1990.
(9) Silvi, B.; Savin, A. *Nature* **1994**, *371*, 683−686.
(10) Silvi, B.; Gatti, C. *J. Phys. Chem. A* **2000**, *104*, 947−953.
(11) Silvi, B. *Phys. Chem. Chem. Phys.* **2004**, *6*, 256−260.
(12) Silvi, B. *J. Phys. Chem. A* **2003**, *107*, 3081−3085.
(13) Kohout, M.; Savin, A. *Int. J. Quantum Chem.* **1996**, *60*, 875−882.
(14) Häussermann, U.; Wengert, S.; Hofmann, P.; Savin, A.; Jepsen, O.; Nesper, R. *Angew. Chem., Int. Ed. Engl.* **1994**, *33*, 2069−2073.
(15) Llusar, R.; Beltrán, A.; Andrés, J.; Noury, S.; Silvi, S. *J. Comput. Chem.* **1999**, *20*, 1517−1526.
(16) Berski, S.; Gutsev, G. L.; Mochena, M. D.; Andres, J. *J. Phys. Chem. A* **2004**, *108*, 6025−6031.
(17) Andres, J.; Berski, S.; Feliz, M.; Llusar, R.; Sensato, F.; Silvi, B. *C. R. Chim.* **2005**, *8*, 1400−1412.
(18) Feliz, M.; Garriga, J. M.; Llusar, R.; Uriel, S.; Humphrey, M. G.; Lucas, N. T.; Samoc, M.; Luther-Davies, B. *Inorg. Chem.* **2001**, *40*, 6132−6138.
(19) *SAINT 6.2*; Bruker Analytical X-ray Systems: Madison, WI, 2001.

Table 1. Crystallographic Data for $Mo_3NiS_4(dmpe)_3Cl_4$

empirical formula	$C_{19.50}H_{49}C_{17}Mo_3NiP_6S_4$
fw	1192.33
cryst syst	cubic
a, Å	16.451(3)
V, Å^3	4452.3(12)
T, K	293(2)
space group	*P*2(1)/3
Z	4
μ (Mo Kα), mm^{-1}	2.081
Θ range, deg	1.75−30.50
reflns collected	37136
unique reflns/R_{int}	4542/0.0698
R1/wR2 ($I > 2\sigma$)[a,b]	0.0363/0.0898
R1/wR2 (all data)[a,b]	0.0512/0.0947
residual ρ/e Å^{-3}	0.880 and −0.677

[a] $R1 = \sum||F_0| - |F_c||/\sum F_0$. [b] $wR2 = [\sum[w(F_0^2 - F_c^2)^2]/\sum[w(F_0^2)^2]]^{1/2}$.

The positions of heavy atoms were determined by using direct methods and successive difference electron-density maps using the SHELXTL software package.[21]

The neutral compound $Mo_3NiS_4(dmpe)_3Cl_4 \cdot 0.5CH_2Cl_2$ crystallizes in the chiral space group $P2_13$ with absolute parameters being refined as 0.04(3). Non-hydrogen atoms of the cluster were refined anisotropically, and the positions of all hydrogen atoms were generated geometrically, assigned isotropic thermal parameters, and allowed to ride on their respective parent carbon atoms. The last Fourier map showed half a dichloromethane molecule which was refined isotropically as a rigid group. The crystal parameters and basic information relating data collection and structure refinement is summarized in Table 1.

Computational Methods. Cluster compounds were optimized at the gradient-corrected density functional theory (DFT) level using the Becke three-parameter hybrid functional (B3LYP)[22] and the same functional with the nonlocal correlation functional provided by Perdew (B3P86),[23] as implemented in the Gaussian 98 program.[24] The geometries of the model compounds $Mo_3NiS_4(PH_3)_6Cl_4$ and $[Mo_3CuS_4(PH_3)_6Cl_4]^+$ were optimized assuming a C_3 symmetry in agreement with the observed X-ray symmetry. Relaxation of the optimization and/or symmetry criteria does show energy differences that affect only the fifth decimal figure. Relativistic compact effective potentials (RCEP) were used to replace the core electrons of Ni, Cu, and Mo (except for the outermost shells) with basis sets splitting {4211/4211/411} (ECP-SBKJC) for the valence and the outmost core electrons.[25] The Mo basis set was customized by applying the generator coordinate method,[26] which prompted us to add an additional d-type diffuse function ($\zeta = 0.143$) on the Mo atom. The corresponding procedure is detailed elsewhere.[27] Valence basis sets for Ni, Cu, and Mo were augmented by a f-type polarization function with the coefficients $\zeta = 3.130$, 3.525, and 1.043, respectively.[28] The 6-31G(d, p) all-electron basis sets were employed for the other atoms.[29,30] Bonding energies were calculated as the difference between optimized energies of each tetrametallic product and the trinuclear $[Mo_3S_4(PH_3)_6Cl_3]^+$, CuCl, and $[NiCl]^-$. Stationary points were characterized by the calculation of vibrational frequencies.

ELF calculations were computed with the TopMod package developed at the Laboratoire de Chimie Théorique de l'Université Pierre et Marie Curie.[31,32] The B3P86 functional was used combined with Ahlrichs triple-ζ basis sets (TZVahl) for Ni and Mo atoms (ftp://ftp.chemie.uni.-karlsruhe.de/pub/basen).[33] The basis sets for the Mo atoms {84211111/641111/51111} were augmented by an f-type polarization function ($\zeta = 1.04835114$). For the Cu and Ni atoms, the basis set {842111/631/411} was augmented by p-type (Cu, $\zeta = 0.155065$; Ni, $\zeta = 0.146588$) and f-type (Cu, $\zeta = 3.55$; N,:$\zeta = 3.04$) polarization functions.[34] The all-electron 6-311G(d, p) basis set was employed for the remaining atoms. All the topological calculations were performed from the geometries optimized at the B3P86/ECP-SBKJC/6-31G(d, p) level. Isosurfaces have been visualized with the public domain scientific visualization and animation program for high-performance graphic workstations named SciAn.[35]

3. Results and Discussion

Synthesis. The trinuclear $[Mo_3S_4(dmpe)_3Cl_3]^+$ complex acts as metalloligand for the preparation of heterodimetallic $Mo_3M'S_4$ clusters.[6,36,37] In the case of copper, reaction of a Cu(I) compound, namely, CuCl or $[Cu(CH_3CN)_4]^+$, results in the formation of $[Mo_3CuS_4(dmpe)_3Cl_4]^+$ in high yields, and the reaction takes place without changes in the formal metal oxidation states.[18] In the case of nickel, no reaction has been observed between $[Mo_3S_4(dmpe)_3Cl_3]^+$ and $NiCl_2$ (also under reducing conditions), and for the reaction to take place the presence of a Ni(0) precursor such as $Ni(cod)_2$ is necessary. When the reaction is done in acetonitrile the final product is $[Mo_3NiS_4(dmpe)_3Cl_3(CH_3CN)]^+$, and reactivity studies show that the acetonitrile ligand can be replaced by CO, sulfur, and nitrogen donor ligands.[6] In this work we

(20) Sheldrick, G. M. *SADABS Empirical Absorption Program*; University of Göttingen: Göttingen, Germany, 1996.
(21) Sheldrick, G. M. *SHELXTL 5.1*; Madison, WI, 1997.
(22) Becke, A. D. *J. Chem. Phys.* **1993**, *98*, 5648−5652.
(23) Perdew, J. P. *Phys. Rev. B* **1986**, *33*, 8822−8824.
(24) Frisch, M. J.; Trucks, G. W.; Schlegel, H. B.; Scuseria, G. E.; Robb, M. A.; Cheeseman, J. R.; Zakrzewski, V. G.; Montgomery, J. A., Jr.; Stratmann, R. E.; Burant, J. C.; Dapprich, S.; Millam, J. M.; Daniels, A. D.; Kudin, K. N.; Strain, M. C.; Farkas, O.; Tomasi, J.; Barone, V.; Cossi, M.; Cammi, R.; Mennucci, B.; Pomelli, C.; Adamo, C.; Clifford, S.; Ochterski, J.; Petersson, G. A.; Ayala, P. Y.; Cui, Q.; Morokuma, K.; Malick, D. K.; Rabuck, A. D.; Raghavachari, K.; Foresman, J. B.; Cioslowski, J.; Ortiz, J. V.; Baboul, A. G.; Stefanov, B. B.; Liu, G.; Liashenko, A.; Piskorz, P.; Komaromi, I.; Gomperts, R.; Martin, R. L.; Fox, D. J.; Keith, T.; Al-Laham, M. A.; Peng, C. Y.; Nanayakkara, A.; Gonzalez, C.; Challacombe, M.; Gill, P. M. W.; Johnson, B.; Chen, W.; Wong, M. W.; Andres, J. L.; Gonzalez, C.; Head-Gordon, M.; Replogle, E. S.; Pople, J. A. *Gaussian 98*, Revision A.7; Gaussian, Inc.: Pittsburgh, PA, 1998.
(25) Stevens, W. J.; Krauss, M.; Basch, H.; Jasien, P. G. *Can. J. Chem.*−*Rev. Can. Chim.* **1992**, *70*, 612−630.
(26) Sensato, F. R.; Custodio, R.; Cass, Q. B.; Longo, E.; Hernandes, M. Z.; Longo, R. L.; Andres, J. *J. Mol. Struct. THEOCHEM* **2002**, *589*, 251−264.
(27) De Souza, H. F.; Guadagnini, P. H.; Custodio, R.; Goddard, J. D. *J. Comput. Chem.* **2000**, *21*, 1119−1131.
(28) Ehlers, A. W.; Bohme, M.; Dapprich, S.; Gobbi, A.; Hollwarth, A.; Jonas, V.; Kohler, K. F.; Stegmann, R.; Veldkamp, A.; Frenking, G. *Chem. Phys. Lett.* **1993**, *208*, 111−114.
(29) Binkley, J. S.; Pople, J. A.; Hehre, W. J. *J. Am. Chem. Soc.* **1980**, *102*, 939−947.
(30) Hehre, W. J.; Ditchfie, R.; Pople, J. A. *J. Chem. Phys.* **1972**, *56*, 2257−2261.
(31) Noury, S.; Krokidis, X.; Fuster, F.; Silvi, B. *TopMod*; Paris, 1997.
(32) Noury, S.; Krokidis, X.; Fuster, F.; Silvi, B. *Comput. Chem.* **1999**, *23*, 597−604.
(33) Ahlrichs, R.; May, K. *Phys. Chem. Chem. Phys.* **2000**, *2*, 943−945.
(34) Wachters, A. J. *J. Chem. Phys.* **1970**, *52*, 1033−1036.
(35) Pepke, E.; Murray, J.; Lyons, J.; Hwu, T.-Z. *SciAn*; Florida State University; Tallahassee, FL, 1993.
(36) Llusar, R.; Uriel, S. *Eur. J. Inorg. Chem.* **2003**, 1271−1290.
(37) Feliz, M.; Llusar, R.; Uriel, S.; Vicent, C.; Coronado, E.; Gomez-Garcia, C. I. *Chem. Eur. J.* **2004**, *10*, 4308−4314.

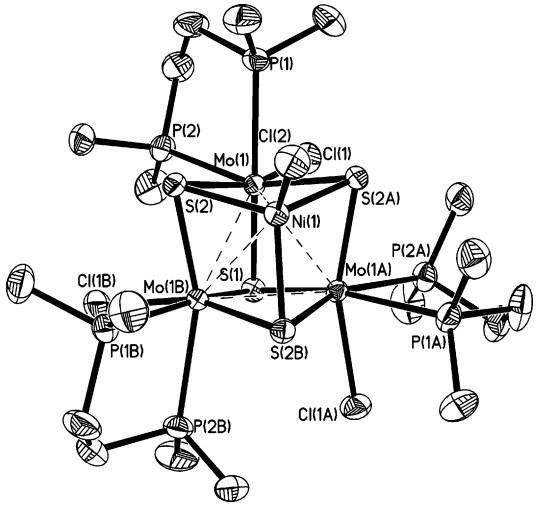

Figure 1. ORTEP representation (50% probability ellipsoids) of the neutral compound $Mo_3S_4Ni(dmpe)_3Cl_4$. Symmetry transformations used to generate equivalent atoms: #A, $z + {}^1/_2$, $-x + {}^3/_2$, $-y + 1$ and #B, $-y + {}^3/_2$, $-z + 1$, $x - {}^1/_2$.

show that acetonitrile is also substituted at room temperature by a halide ligand by reacting $[Mo_3NiS_4(dmpe)_3Cl_3(CH_3CN)]^+$ with an excess of TBACl in presence of a noncoordinating solvent to afford the neutral $Mo_3NiS_4(dmpe)_3Cl_4$ compound. This neutral complex can be directly compared with the already reported $[Mo_3CuS_4(dmpe)_3Cl_4]^+$ compound due to the similarities between their coordination environments and metal electron count (16 metal electrons), which allows a study of the influence of the heterometal on the physicochemical properties of the cluster.

There are significant differences regarding the M′ insertion into the trinuclear Mo_3S_4 unit, and these are reflected in the final properties of the heterodimetallic cluster. In this context, we have studied the molecular and electronic structure of two isoelectronic cluster complexes, namely, $[Mo_3CuS_4(dmpe)_3Cl_4]^+$ and $Mo_3NiS_4(dmpe)_3Cl_4$. When appropriate, their properties have been compared with those of their trinuclear precursor $[Mo_3S_4(dmpe)_3Cl_3]^+$. We have started our investigation with the clusters' geometry optimization and further comparison between the experimental and theoretical bond distances and angles. Calculated vibrational frequencies have also been compared with experimental values aimed to validate the electronic structure, and the results are presented in the next section.

Structure. The neutral $Mo_3NiS_4(dmpe)_3Cl_4$ compound crystallizes in the cubic noncentrosymmetric space group $P2_13$ from a racemic mixture of $[Mo_3NiS_4(dmpe)_3Cl_3(CH_3CN)]^+$ in dichloromethane in the presence of an excess of a halide salt. There is a preferential crystallization of one of the enantiomers, and its structural analyses confirms the presence of a cubane-type Mo_3NiS_4 cluster core with its innermost part formed by a tetrahedral arrangement of three molybdenum atoms and one nickel atom. Each tetrahedral face is capped by a μ_3-coordinated sulfido ligand, thus generating the cubane-like structure, as represented in Figure 1. The molybdenum atoms have an octahedral configuration (if metal−metal bonds are neglected) formed by three sulfur atoms, two phosphorus atoms from the dmpe ligand, and one halogen atom. The coordination of the diphosphine with one phosphorus atoms trans to sulfur and the other trans to chloride results in chiral clusters. The ligand environment around the heterometal, Ni or Cu, is tetrahedral.

Table 2. Calculated and X-ray Interatomic Distances (angstrom) for $Mo_3M'S_4$ (M′ = Ni, Cu) Clusters Coordinated to Phosphanes

	$[Mo_3CuS_4(diphos)_3Cl_4]^+$		$Mo_3NiS_4(diphos)_3Cl_4$	
distances	B3P86[a]	exptl[b]	B3P86[a]	exptl[c]
Mo−Mo	2.762	2.782[1]	2.758	2.8104(7)
Mo−M	2.839	2.823[2]	2.647	2.6844(9)
Mo−S(1)	2.368	2.370[2]	2.376	2.3744(14)
Mo−S(2)	2.383	2.361[2]	2.391	2.3675(11)
Mo−S(2)	2.331	2.320[3]	2.345	2.3355(11)
M−S(2)	2.324	2.305[2]	2.213	2.2147(11)
Mo−Cl	2.446	2.473[13]	2.495	2.5424(12)
Mo−P(1)	2.538	2.536[4]	2.517	2.5527(13)
Mo−P(2)	2.580	2.590[5]	2.560	2.5804(13)
M−Cl	2.147	2.1798(16)	2.188	2.235(2)

[a] Diphosphane replaced by two PH_3's in each $Mo_3M'S_4$ cluster. [b] Average bond distances taken from the $[Mo_3CuS_4(dmpe)_3Cl_4]^+$ X-ray structure. See ref 18. [c] Average bond distances taken from the $Mo_3NiS_4(dmpe)_3Cl_4$ X-ray structure reported in this work.

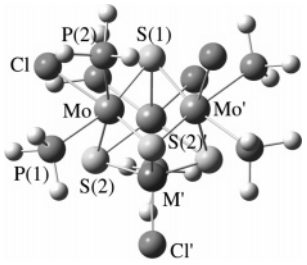

Figure 2. Structure of the model cubane $[Mo_3M'S_4(PH_3)_6Cl_4]^n$ (M′ = Cu, $n = +1$; M′ = Ni, $n = 0$) cluster.

The intermetallic distances are consistent with the presence of metal−metal single bonds, and the incorporation of the nickel atom in the trinuclear $[Mo_3S_4(dmpe)_3Cl_3]^+$ cluster produces an elongation of the Mo−Mo average bond distance from 2.766 to 2.810 Å. The Mo−Ni bond lengths are 0.13 Å shorter than the Mo−Mo distances. Table 2 presents a list of selected X-ray bond distances for $Mo_3NiS_4(dmpe)_3Cl_4$ and its isolectronic copper complex together with the optimized distances calculated for the model cluster compounds $[Mo_3M'S_4(PH_3)_6Cl_4]^{0/+}$, represented in Figure 2. Two functionals, namely, B3P86 and B3LYP, have been used in the computational study, and the results are given as Supporting Information. B3P86 results have been chosen for further discussions due to the good agreement with the experimental and optimized structural parameters, as represented in Table 2.

The optimized intermetallic bond lengths follow the experimental trends with a Mo−Cu distance considerably longer, by ca. 0.2 Å, than the corresponding Mo−Ni bond length (see Table 2). Among the Mo−(μ_3-S) bond distances, where the sulfur ligand is that capping the Mo_2M' face, those trans to the phosphorus atom are 0.05 Å longer than the other ones. This observation is attributed to the stronger trans influence of the phosphane versus the chloride ligand, and this tendency is also reflected in the optimized Mo−S bond lengths. In general, optimized metal−metal and metal ligand

Table 3. Selected Vibrational Calculated and Experimental Frequencies (cm^{-1}) of Mo_3S_4 and $Mo_3M'S_4$ (M′ = Ni, Cu) Clusters Coordinated to Phosphanes

Vibrational modes		$[Mo_3S_4(diphos)_3Cl_3]^+$		$[Mo_3CuS_4(diphos)_3Cl_4]^+$		$Mo_3NiS_4(diphos)_3Cl_4$	
		calc [a]	exptl [b]	calc [a]	exptl [b]	calc [a]	exptl [b]
A, *bending*	Raman	190	185	271	264	290	-
A, *stretching*	Raman	345	351	347	352	338	-
A, *stretching*	Raman	-	-	376	384	373	-
A, *stretching*	IR	430	423	416	415	414	410
	Raman	-	430	-	412	-	-
E, *bending*	IR	447	440	433	440	433	430
	Raman	-	433		433	-	-
A, *stretching*	IR	472	475	466	467	458	438
	Raman	-	475	-	469	-	-

[a] Diphosphane replaced by two PH_3's in Mo_3S_4 and $Mo_3M'S_4$ clusters. [b] Diphosphane replaced by dmpe in each Mo_3S_4 and $Mo_3M'S_4$ cluster.

bond distances in these tetrametallic cuboidal clusters reproduce experimental trends, as previously observed for their trinuclear cluster precursor.[38] The higher deviations correspond to the Mo−Mo and Mo/M′-Cl bonds, with maximum values of 0.05 Å.

In order to validate the optimized structures, their Raman and IR frequencies have been computed and compared with the measured experimental spectra. Several combined DFT and pseudopotential vibrational studies have shown a good agreement between calculated and experimental data.[26,39] Table 3 outlines the calculated and experimental IR and Raman frequencies for the $Mo_3M'S_4$ (M′ = Ni or Cu) cores, together with their corresponding vibrational modes. Spectroscopic results for Mo_3S_4 have been included for comparison.

Computed frequencies associated to the stretching Mo−Mo modes do not vary substantially on going from Mo_3S_4 to $Mo_3M'S_4$. However, significant differences are seen in A bending frequencies where heterometal coordination causes a Raman frequency increase from 190 cm^{-1} in the trinuclear complex to 271 and 290 cm^{-1} in the Mo_3CuS_4 and Mo_3NiS_4 clusters, respectively. This is the first theoretical study using ab initio methodologies aimed to identify the different vibrational modes within these cubane-type cluster cores. Other methodologies based on the valence force field approximation have been employed, and they have presented some deficiencies as the significantly low computed Mo−Mo frequency (200 cm^{-1}) compared with experimental values for Mo_3S_4 and Mo_3S_7 clusters.[40,41] However, the calculated Mo−(μ_3-S) IR stretching frequency for $[Mo_3S_{13}]^{2-}$ (462 cm^{-1}) using these methodologies matches the frequency computed in this work for $[Mo_3S_4(PH_3)_6Cl_3]^+$ (472 cm^{-1}).[41] In general we can state that for Mo_3S_4 and $Mo_3M'S_4$ computed vibrational frequencies agree with experimental values within experimental error (0−7%).

Energetics. The shorter Mo−M′ distances measured and calculated for nickel in comparison with copper are indicative of a stronger interaction between the Mo_3S_4 fragment and the M′-Cl subunit in the case of nickel. The more robust nature of the Mo_3NiS_4 fragment is also confirmed by mass spectrometry experiments where the tetrametallic cluster unit remains intact at high collision energies (up to 40 eV). In contrast, for the copper containing cluster evolution of one diphosphine ligand is accompanied by the loss of a "CuCl" fragment to give $[Mo_3S_4Cl_3(dmpe)_2]^+$ at these energy values. For the nickel cluster, fragmentation of the heterometal is only observed at collision energies of 60 eV.[42]

The Mo_3−M′Cl bond dissociation energies associated to the $[Mo_3M'S_4(PH_3)_6Cl_4]$ (M′ = Ni or Cu) products show that the calculated value for copper (34 kcal/mol) is significantly lower than that of the nickel (169 kcal/mol) compound, in agreement with the shorter Mo−M′ bond distances and the higher robustness of the Mo_3NiS_4 unit as inferred from mass spectrometry investigations. These facts together with the changes in the redox behavior observed upon Ni incorporation are indicative of an electron-donor character of the Ni−Cl fragment upon coordination to the Mo_3S_4 unit, and this circumstance should be reflected in changes in the electron density distribution. In order to investigate this hypothesis, the XPS spectra of the trimetallic and tetrametallic complexes have been measured and their values compared with the atomic charges populations based on topological approaches.[17]

Oxidation States. The XPS spectra of the Mo3d lines of the complexes $[Mo_3S_4(dmpe)_3Cl_3]^+$, $[Mo_3CuS_4(dmpe)_3Cl_4]^+$, and $Mo_3NiS_4(dmpe)_3Cl_4$ are shown in Figure 3, and the Cu 2p and Ni 2p lines of the corresponding $[Mo_3CuS_4(dmpe)_3Cl_4]^+$ and $Mo_3NiS_4(dmpe)_3Cl_4$ complexes are displayed in Figure 4, parts a and b, respectively. The binding energies

(38) Feliz, M.; Llusar, R.; Andres, J.; Berski, S.; Silvi, B. *New J. Chem.* **2002**, *26*, 844−850.
(39) Dimitrova, Y.; Slavova, I. *Spectrochim. Acta, Part A* **2005**, *61*, 2095−2102.
(40) Basova, T. V.; Kolesov, B. A.; Samsonenko, D. G.; Fedin, V. P. *Russ. J. Inorg. Chem.* **2000**, *45*, 1098−1104.
(41) Fedin, V. P.; Kolesov, B. A.; Mironov, Y. V.; Fedorov, V. Y. *Polyhedron* **1989**, *8*, 2419−2423.
(42) Guillamón, E.; Llusar, R.; Pozo, O.; Vicent, C. *Int. J. Mass Spectrom.* **2006**, *254*, 25−33.

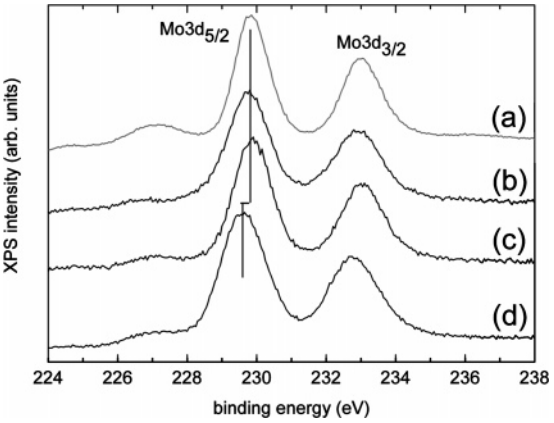

Figure 3. XPS spectra of the Mo 3d lines of (a) MoS_2, (b) $[Mo_3S_4(dmpe)_3Cl_3]PF_6$, (c) $[Mo_3CuS_4(dmpe)_3Cl_4]PF_6$, and (d) $Mo_3NiS_4(dmpe)_3Cl_4$.

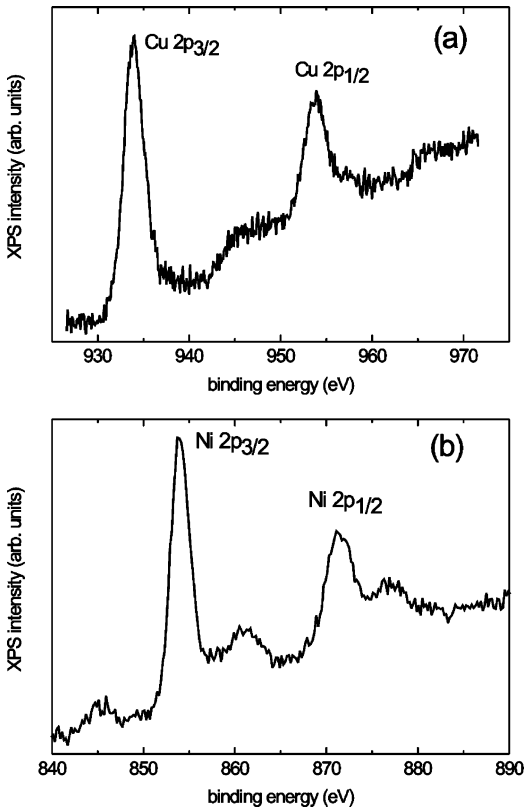

Figure 4. XPS spectra of (a) the Cu 2p lines of $[Mo_3CuS_4(dmpe)_3Cl_4]PF_6$ and (b) the Ni 2p lines of $Mo_3NiS_4(dmpe)_3Cl_4$.

of the Mo $3d_{5/2}$ line are 229.8, 229.9, and 229.6 eV for $[Mo_3S_4(dmpe)_3Cl_3]PF_6$ (Figure 3b), $[Mo_3CuS_4(dmpe)_3Cl_4]PF_6$ (Figure 3c), and $Mo_3NiS_4(dmpe)_3Cl_4$ (Figure 3d), respectively. These lines are compared to the XPS spectra of MoS_2 (Figure 3a), a reference material with a nominal Mo(IV) oxidation state (229.8 eV). Note that for $[Mo_3S_4(dmpe)_3Cl_3]^+$ and $[Mo_3CuS_4(dmpe)_3Cl_4]^+$ the formal oxidation state of Mo is +IV, while the insertion of Ni into $[Mo_3S_4(dmpe)_3Cl_3]^+$ induces a small but reproducible decrease of 0.3 eV suggesting a reductive addition of nickel into the trinuclear cluster. In the case of $[Mo_3CuS_4(dmpe)_3Cl_4]PF_6$ (Figure 4a), the Cu 2p line position and satellite structure strongly indicate that the oxidation state of copper corresponds to Cu(I), thus

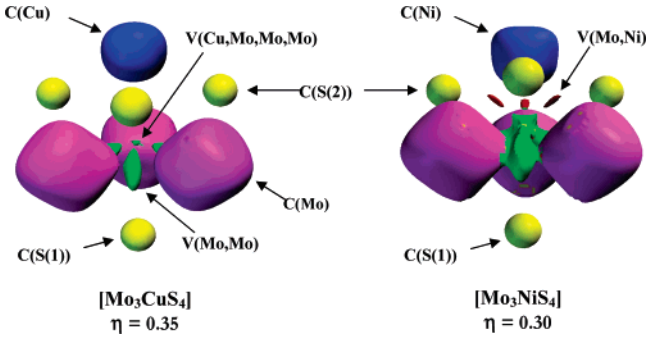

Figure 5. Simplified valence and core attractor representation of the $Mo_3M'S_4$ (M′ = Cu, Ni) units at each ELF value. Color code for each attractor: C(S), yellow; C(Mo), magenta; C(M′), blue; V(Mo, Mo), green; V(Mo, Ni), red; V(Cu, Mo, Mo, Mo), green.

corresponding to a closed d-shell configuration. This result is in line with previously reported XPS measurements performed with $[Mo_3CuS_4(Hnta)_3Cl]^{2-}$.[43]

The XPS spectrum of the Ni 2p line of $Mo_3NiS_4(dmpe)_3Cl_4$ is depicted in Figure 4b. The binding energy of Ni $2p_{3/2}$ is 854.0 eV, with a spin−orbit splitting of 17.5 eV. The satellite features around 862 and 877 eV indicate the presence of electron correlations in the system (Coulombic repulsion, charge transfer, etc.) and can be interpreted in terms of contributions from various electron configurations to the ground state wave function (open d-shell configuration), namely, d^8, d^9L^1, and $d^{10}L^2$ where L represents the ligand attached to nickel (sulfur in this complex), corresponding to a formal Ni(II) oxidation state.[44] From the experimental data one cannot assess which configuration, d^8, d^9L^1, or $d^{10}L^2$, dominates, that is, which corresponds to the main Ni $2p_{3/2}$ peak and which to the satellites and would require configuration interaction calculations. Note that different electronic configurations are observed with XPS since photoemission is an intrinsically rapid process, giving a dynamical view of the electronic structure.[45]

In this work, topological methodologies have been used to evaluate the electronic distribution in these systems. The topological analysis of the ELF gradient field constitutes an alternative to the AIM use of electron density as the potential function. Such analysis allows recovering chemical objects as atoms, bonds, and lone pairs associated to the different basins which are significant in chemistry. A topological analysis of the ELF isosurface for $Mo_3M'S_4$ units identifies the four following irreducible domains assigned to the S(1) and S(2) sulfur valence shell, V(Mo−S) and V(S), as found for the Mo_3S_4 cluster unit plus a reducible metallic Mo_3M' superbasin.[17] No disynaptic V(M′, S) basin is observed in any case. ELF topology shows that the Mo_3Cu cluster unit behaves as an entity, in a similar way to the Mo_3 core in $[Mo_3S_4(dmpe)_3Cl_3]^+$, and its bonding arises from the presence

(43) Akashi, H.; Shibahara, T. *Inorg. Chim. Acta* **2000**, *300*−*302*, 572−580.
(44) Krishnakumar, S. R.; Shanthi, N.; Mahadevan, P.; Sarma, D. D. *Phys. Rev. B* **2000**, *61*, 16370−16376.
(45) For a discussion on the electronic structure of materials containing transition metals with XPS see, e.g., Muñoz-Rojas, D.; Subías, G.; Fraxedas, J.; Gómez-Romero, P.; Casañ-Pastor, N. *J. Phys. Chem. B* **2005**, *109*, 6193−6203 and references therein.

Table 4. Basin Populations (N, [e$^-$]), Variances (σ^2, [e$^-$]^2), and Atomic Contributions to Each Basin ([e$^-$]) of Mo_3S_4 and $Mo_3M'S_4$ (M′ = Ni, Cu) Clusters Coordinated to Phosphanes

	$[Mo_3S_4(PH_3)_6Cl_3]^+$			$[Mo_3CuS_4(PH_3)_6Cl_4]^+$			$Mo_3NiS_4(PH_3)_6Cl_4$		
basin	N	σ^2	atomic contributions	N	σ^2	atomic contributions	N	σ^2	atomic contributions
V(M′, Mo, Mo, Mo)				0.36	0.54	Mo, 0.08 × 3; Cu, 0.12	0.25	0.23	Mo, 0.05 × 3; Ni, 0.11
V(Mo, Mo, Mo)	0.16	0.16	Mo, 0.05 × 3						
V(Mo, Mo)	0.42	0.38	Mo, 0.20 × 2	0.45	0.40	Mo, 0.22 × 2	0.46	0.42	Mo, 0.25 × 2
V(Mo, M′)							0.21	0.20	Mo, 0.08; Ni, 0.12
V(Mo, S(1))	1.43	1.00	Mo, 0.26; S(1), 1.15	1.46	1.00	Mo, 0.26; S(1), 1.18	1.47	1.00	Mo, 0.26; S(1), 1.22
V(Mo, S(2))	1.05	0.78	Mo, 0.23; S(2)′ 0.81	1.55	1.06	Mo, 0.28; S(2), 1.23; Cu, 0.04	1.58	1.08	Mo, 0.27; S(2), 1.26; Ni, 0.04
V(Mo, S(2)′)	1.27	0.90	Mo, 0.24; S(2), 1.00	1.72	1.15	Mo, 0.23; S(2)′, 1.37; Cu, 0.04	1.65	1.12	Mo, 0.26; S(2)′, 1.35; Ni, 0.04
V(S(2))	4.83	1.95	Mo, 0.10; S(2), 4.64	4.08	1.81	Cu, 0.16; S(2), 3.89	4.13	1.80	Ni, 0.21; S(2), 3.93
V(Mo, Cl)	0.62	0.51	Mo, 0.10; Cl, 0.51	0.64	0.52	Mo, 0.10; Cl, 0.54	0.75	0.60	Mo, 0.10; Cl, 0.65
V(Mo, P(1))	1.99	1.10	Mo, 0.26; P(1), 1.73	1.96	1.08	Mo, 0.26; P(1), 1.70	2.00	1.10	Mo, 0.25; P(1), 1.75
V(Mo, P(2))	1.97	1.07	Mo, 0.23; P(2), 1.72	1.96	1.09	Mo, 0.24; P(2), 1.71	2.00	1.09	Mo, 0.24; P(2), 1.76
C(Mo)	38.87	2.50	Mo, 38.87	38.88	2.50	Mo, 38.88	38.96	2.54	Mo, 38.96
C(M′)				27.10	1.41	Cu, 27.10	25.99	2.05	Ni, 25.99
V(S(1))	2.92	1.37	S(1), 2.91	2.89	1.35	S(1), 2.88	2.87	1.34	S(1), 2.86
V(Cl)	3.82	1.64	Mo, 0.03; Cl, 3.78	3.47	1.60	Cl, 3.41	3.85	1.63	Cl, 3.83
V(Cl)	3.38	1.52	Mo, 0.03; Cl, 3.36	3.96	1.54	Cl, 3.69	3.25	1.48	Cl, 3.23
V(Cl)[a]				2.70	1.37	Cl, 2.55; Cu, 0.15	2.44	1.25	Cl, 3.38; Ni, 0.05

[a] Three monosynaptic $V(Cl)_{M'}$ basins of the chlorine attached to the heterometal were obtained.

of a tetrasynaptic V(M′, Mo, Mo, Mo) plus three disynaptic V(Mo, Mo) basins, as represented in Figure 5. In the case of the nickel complex, one tetrasynaptic V(Ni, Mo, Mo, Mo) and three disynaptic V(Mo, Ni) basins are also identified. Table 4 lists the basin populations, covariances, and atomic contributions for each basin.

We had previously presented a discussion of the basin populations upon insertion of the M′−Cl subunit into the Mo_3S_4 cluster core to conclude that the molybdenum core population (ca. 38.9 e$^-$) does not show significant differences in going from the trinulear to the tetranuclear cluster for both copper and nickel.[17] This population analysis also shows that the $Mo_3M'S_4$ core behaves as a unique chemical entity, an observation supported by mass spectrometry experiments and chemical reactivity studies on these cluster complexes, i.e., substitution of the CH_3CN molecule coordinates to nickel by a chloride ligand. The total population of the Mo_3M' superbasin is 1.71 e$^-$ for the copper complex and 2.26 e$^-$ for the nickel compound in front of the value of 1.42 e$^-$ computed for the Mo_3 trinuclear precursor at the same level of calculation; therefore, there is a higher electron transfer in the case of nickel as predicted from the XPS experimental investigations.

On the other hand, the calculated population for the copper and nickel cores are 27.10 and 25.99 e$^-$, respectively. These numbers suggest an M′(II) oxidation state for the metal, but only latter population would enter in agreement with the XPS experiments. However, one should also consider the population of the metallic Mo_3M' superbasin and also the covariance of a certain basin population. Higher covariances are indicative of electron delocalization at the same time than support the phenomenological interpretation of the electron density in terms of mesomeric structures. For the complexes under investigation the covariance of the metallic basins, namely, the core C(M′) and the metallic Mo_3M' superbasin, comes basically from the V(S(2)) lone pairs. In particular, the covariance of the C(Ni) is 2.05 e^2 versus the 1.41 e^2 calculated for C(Cu). The high covariances calculated for the basin electron populations are an unequivocal signal of the ambiguous character of the formal oxidation states in these kinds of complexes. The most intense peak in the $Mo_3NiS_4(dmpe)_3Cl_4$ XPS spectra corresponds to the dominant mesomeric structure, and the presence of satellite peaks in the XPS spectra can be due to the higher covariances calculated for this system. At the moment it is not possible to draw a line between "oxidation state precise" cluster complexes such as $[Mo_3CuS_4(dmpe)_3Cl_4]^+$ and the nonprecise systems due to the small differences in the covariance-calculated values. However, we can conclude that electron density distributions in compounds with high electron population covariances can be conveniently expressed using mesomeric structures, and simplified related concepts such as "formal oxidation states" should take into account this fact.

4. Conclusion

Structural, spectroscopic, energetic, and electronic changes associated to the insertion of a heterometal, Cu or Ni, into the incomplete cuboidal Mo_3S_4 unit have been calculated using ab initio methodologies and the results compared with experimentally determined values. In spite of the good agreement between theory and experiment found for these systems, the answer regarding the metal formal oxidation states assignment still remains inconclusive. We attribute this fact to the electronic delocalization present in these cluster complexes. Such delocalization is reflected in the XPS spectra line shape and the high topological covariances calculated for the metallic basins.

Acknowledgment. The financial support of the Spanish Ministerio de Educación y Ciencia (research project BQU2003-03194) and the EU FEDER Program (Grant CTQ2005-09270-C02-01), Fundació Bancaixa-UJI (research project

P1.1B2004-19) and Generalitat Valenciana (research project ACOMP06/241) is gratefully acknowledged. The authors also thank the Servei Central D'Instrumentació Cientifica (SCIC) of the Universitat Jaume I for providing us with the mass spectrometry and X-ray facilities. F.S. thanks the Fundació Caixa Castelló −UJI for financing his stay as a postdoctoral fellow at the Universitat Jaume I.

Supporting Information Available: X-ray crystallographic file in CIF format of $Mo_3NiS_4(dmpe)_3Cl_4$ and PDF file of optimized bond distances and angles for the model compounds $[Mo_3CuS_4(PH_3)_6Cl_4]^+$ and $Mo_3NiS_4(PH_3)_6Cl_4$ using B3LYP and BPP86 methodologies. This material is available free of charge via the Internet at http://pubs.acs.org.

IC061853G